Supplementary Information: Precise molecular ordering in discotic monolayers through supramolecularnanoarchitectonics

Himangshu Paul,[†] Priyanka Priyadarshani Samal,[†] Nishant Kumar,[†] Ritobrata De,[‡] Joydip De,[‡] Santanu Kumar Pal,[‡] Puneet Mishra,[*,¶] and Alpana Nayak[*,†]

[†]*Department of Physics, Indian Institute of Technology Patna, Patna-801106, India*

[‡]*Department of Chemical Sciences, Indian Institute of Science Education and Research (IISER) Mohali-140306, India.*

[¶]*Department of Physics, Mahanth Madhusudan College, Patliputra University, Bikram, Patna-801104, India*

E-mail: puneet.physics@gmail.com; anayak@iitp.ac.in

S1. Experimental and Computational Methods

Synthesis and Characterization

The heterocoronene-based discotic liquid crystalline (DLC) molecules, namely the parent heterocoronene (HET) and the oxadiazole-integrated heterocoronene (HET-OXD), were synthesized following previously reported procedures.[1,2] Both compounds were purified by column chromatography and characterized by ^{1}H NMR, ^{13}C NMR, FT–IR, and elemental analysis, confirming their chemical identity and high purity. The molecular geometries were initially optimized using the MMFF94 force field as implemented in MarvinSketch to estimate molecular projection areas. Electronic structure calculations were carried out using density functional theory (DFT) at the B3LYP/6-31G(d) level to obtain optimized geometries and gas-phase dipole moments. For HET-OXD, the optimized dipole moment was found to be 8.45 D oriented at approximately 79.6° with respect to the heterocoronene basal plane, while for HET the dipole magnitude was 4.95 D at 76.4°. The projection area of the core for the HET-OXD (including the oxadiazole moeity) and HET DLC were calculated using Marvin software.[3]

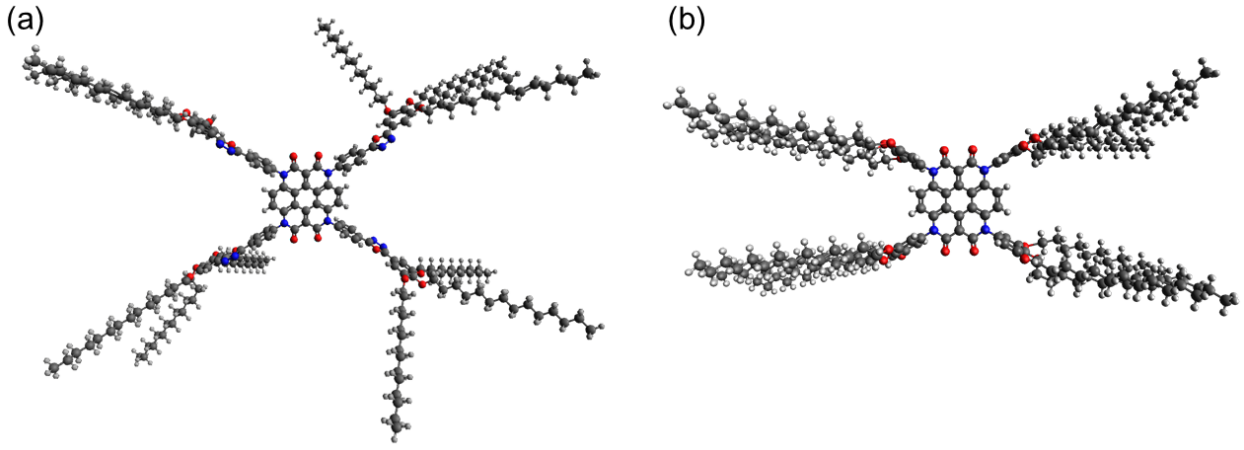

Figure S1: DFT optimized structure of (a) HET-OXD and (b) HET.

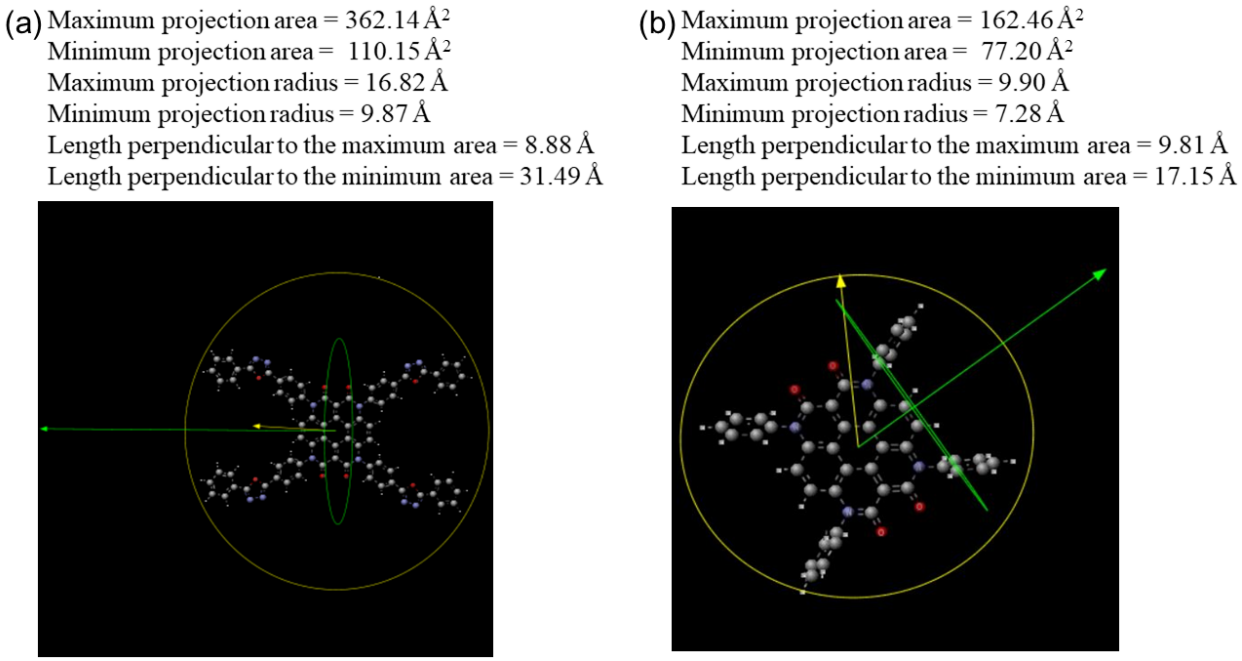

Figure S2: Projection area of (a) HET-OXD and (b) HET.

Langmuir Film Preparation and Characterization

Monolayers of HET and HET-OXD were prepared at the air–water interface using a NIMA 611M Langmuir trough. Chloroform solutions (100 µM) of the compounds were spread onto ultrapure water at room temperature and allowed to equilibrate for 10 min before compression. Surface pressure–area (Π–A) isotherms were recorded at a barrier speed of 10 mm min^{-1}. Simultaneously, surface potential (ΔV) measurements were performed using a vibrating plate Kelvin probe mounted above the film surface. Real-time Brewster angle microscopy (BAM) images were captured using a KSV-NIMA MicroBAM instrument, enabling visualization of domain morphology during compression. Langmuir–Blodgett (LB) transfer was carried out onto Si(100) at the desired surface pressures. The transferred films were characterized by atomic force microscopy (AFM) in tapping mode using a Bruker Multimode 8 system. AFM images were processed and analyzed using WSxM software.[4] ATR–FTIR measurements were performed using a PerkinElmer spectrometer (Model LR649 12C) operated in attenuated total reflection (ATR) mode.

Data Analysis and Fitting Procedure

The surface-pressure $\Pi(A)$ and surface-potential $\Delta V(A)$ isotherms were analyzed jointly using nonlinear least-squares fitting based on logistic formalism. All analyses were performed in Python (version 3.11, Anaconda distribution) using the `lmfit` package. The fitting employed a coupled model in which the mechanical and electrical responses share common structural parameters ($A_{c,P}$, $A_{t,P}$, f_0, and α_m), ensuring thermodynamic consistency between $\Pi(A)$ and $\Delta V(A)$.

For the potential component, the model implemented the orientational relations $\mu_\perp(A) = \mu \sin[\theta(A)]$ and $\sigma_\mu(A) = f(A)\mu_\perp(A)/A$, combined with the Helmholtz expression $\Delta V(A) = V_0 + \sigma_\mu(A)/(\varepsilon_0 \varepsilon_{\text{eff}}) \times 10^{20}$. Two functional forms were tested for the orientational transition: (i) a symmetric logistic form ($\beta = 1$) and (ii) an asymmetric stretched-logistic form with an additional exponent $\beta > 1$ to capture cooperative effects.

The best-fit parameters were obtained by minimizing the combined residuals of $\Pi(A)$ and $\Delta V(A)$ using a Levenberg–Marquardt algorithm. Parameter uncertainties represent one standard deviation estimated from the covariance matrix of the fitted parameters.

S2. Surface roughness as a function of scan size at different transfer pressures

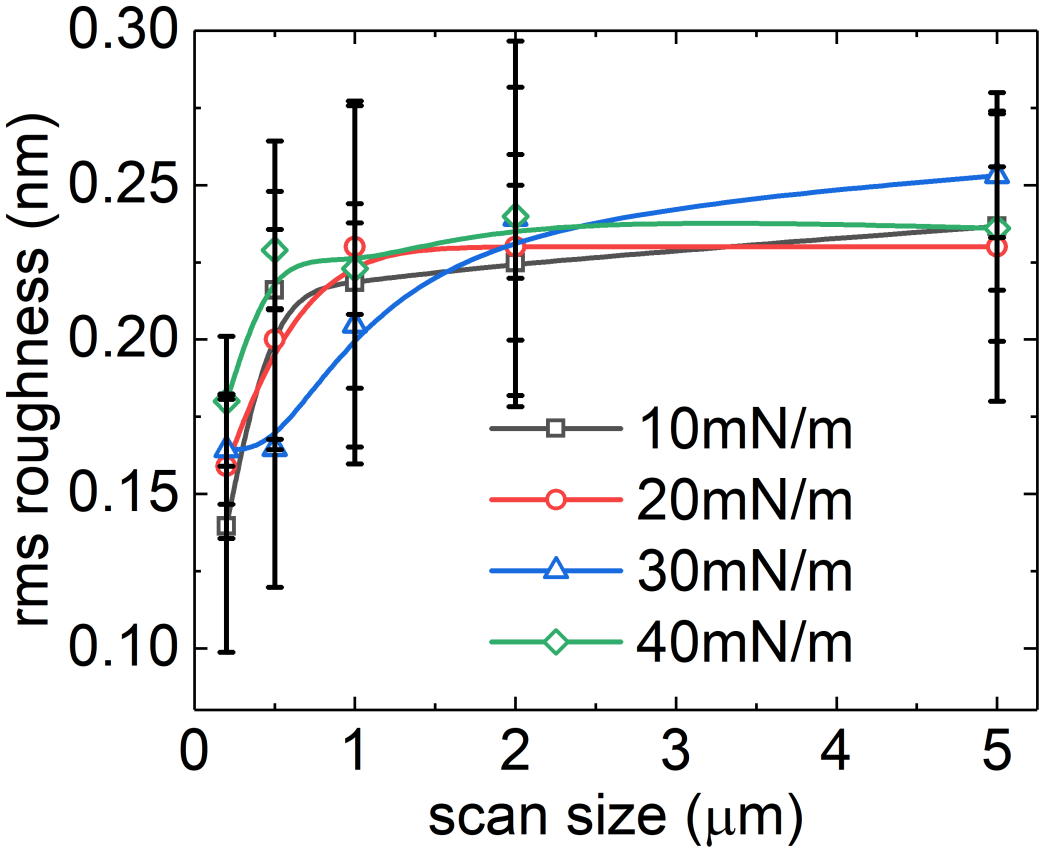

Figure S3: Variation of the RMS roughness with AFM scan size for HET-OXD monolayers transferred onto Si substrates at different surface pressures. A spline curve is included as a guide to the eye.

S3. Film thickness as a function of transfer pressure for HET-OXD

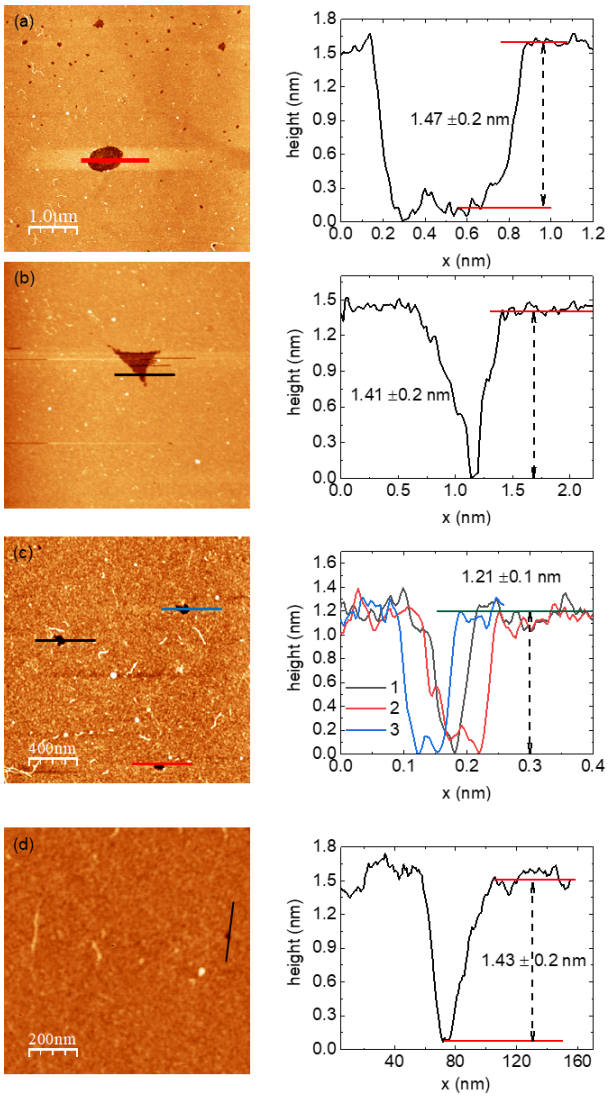

Figure S4: AFM height images of HET–OXD monolayers transferred onto Si substrates at surface pressures of (a) 10, (b) 20, (c) 30, and (d) 40 mN/m. Film thickness was determined from step heights measured across naturally occurring holes or defects in the monolayer. The corresponding height profiles for each pressure are shown to the right of the images.

S4. ATR–FTIR analysis of Langmuir–Blodgett films

To provide additional insight into molecular interactions and packing within the transferred monolayers, attenuated total reflection Fourier-transform infrared (ATR–FTIR) spectra were recorded for Langmuir–Blodgett (LB) films of HET and HET–OXD transferred at a surface pressure of 10 $\mathrm{mN\,m^{-1}}$. The comparison focuses on the 1500–1600 $\mathrm{cm^{-1}}$ spectral region, which is dominated by in-plane aromatic C=C stretching vibrations of the heterocoronene core and is known to be sensitive to electronic polarization and intermolecular coupling.

As shown in Figure SS5, the HET LB film exhibits prominent bands at approximately 1505 and 1538 $\mathrm{cm^{-1}}$. Upon incorporation of the oxadiazole unit, both bands shift systematically to higher wavenumbers in the HET–OXD film. Such blue shifts may suggest stiffening of the corresponding vibrational modes, consistent with increased electronic polarization of the aromatic framework and enhanced intermolecular constraints arising from dipole–dipole interactions in the condensed monolayer. In contrast, the band at approximately 1560 $\mathrm{cm^{-1}}$ appears at the same position in both films, suggesting that the fundamental heterocoronene core remains structurally intact and that the electronic perturbation induced by oxadiazole functionalization is selective rather than global. The selective nature of the observed shifts indicates that oxadiazole incorporation modifies local electronic structure and intermolecular coupling without inducing significant distortion of the aromatic backbone.

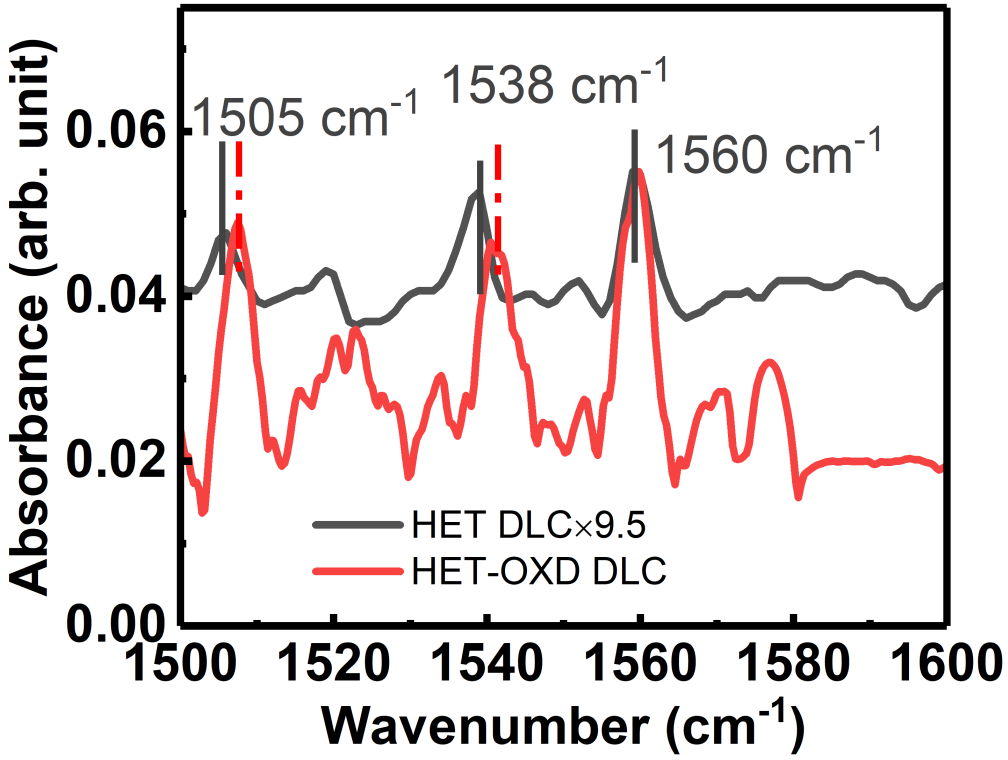

Figure S5: ATR–FTIR spectra of Langmuir–Blodgett films of HET and HET–OXD transferred at a surface pressure of 10 mN m^{-1}. The spectra are shown in the 1500–1600 cm^{-1} region, highlighting aromatic C=C stretching modes of the heterocoronene core. The HET spectrum is scaled by a factor of 9.5 for clarity. The bands at approximately 1505 and 1538 cm^{-1} shift to higher wavenumbers upon oxadiazole functionalization, whereas the band at approximately 1560 cm^{-1} remains unchanged, indicating selective electronic perturbation of the aromatic framework without disruption of the core structure.

S5. Joint Fitting Framework

The experimental surface-pressure $\Pi(A)$ and surface-potential $\Delta V(A)$ isotherms were jointly fitted using a custom Python 3.11 script developed within the Anaconda Spyder IDE. The nonlinear optimization was carried out using the `lmfit` package (version 1.2.2), which wraps the Levenberg–Marquardt algorithm and provides parameter correlation and uncertainty estimates.

Functional forms

The logistic model is defined as

$$\Pi(A) = \Pi_{\min} + \frac{\Pi_{\max} - \Pi_{\min}}{1 + \exp\left(\frac{A - A_{c,P}}{A_{t,P}}\right)},$$

and

$$S_V(A) = \frac{1}{\left[1 + \exp\left(\frac{A - A_{c,V}}{A_{t,V}}\right)\right]^{\beta}},$$

with $\beta = 1$ for the pure logistic case and $\beta > 1$ for the stretched logistic form. The instantaneous dipole tilt is expressed as

$$\theta(A) = \theta_0 + \Delta\theta\, S_V(A),$$

and the normal component of the dipole moment and its surface density are

$$\mu_\perp(A) = \mu \sin[\theta(A)], \qquad \sigma_\mu(A) = \frac{f(A)\,\mu_\perp(A)}{A},$$

where

$$f(A) = f_0 \left[1 - \alpha_m \exp\left(-\frac{A_{c,P} - A}{A_m}\right)\right].$$

The surface potential follows the Helmholtz relation:

$$\Delta V(A) = V_0 + \frac{\sigma_\mu(A)}{\varepsilon_0\, \varepsilon_{\text{eff}}} \times 10^{20}.$$

Parameter initialization and bounds

Initial guesses for $A_{c,P}$, $A_{t,P}$, and $\Pi_{\max}$ were estimated directly from the experimental $\Pi(A)$ curve. The dielectric constant ε_{eff} was fixed at 2.4 based on reported values for aromatic

monolayers. Reasonable physical bounds were applied:

$$0 < f_0 \leq 1, \quad 0 \leq \alpha_m \leq 1, \quad A_m > 0, \quad A_{t,V}, A_{t,P} > 0, \quad 0 < \varepsilon_{\text{eff}} < 5.$$

The stretching exponent β was restricted to $1 \leq \beta \leq 20$. All other parameters were allowed to vary freely.

Joint fitting strategy

The objective function minimized the combined residuals of $\Pi(A)$ and $\Delta V(A)$:

$$\chi^2 = \sum_i \left[\frac{\Pi_{\text{exp}}(A_i) - \Pi_{\text{fit}}(A_i)}{\sigma_{\Pi,i}} \right]^2 + \sum_j \left[\frac{\Delta V_{\text{exp}}(A_j) - \Delta V_{\text{fit}}(A_j)}{\sigma_{V,j}} \right]^2.$$

Equal weights were assigned to the two datasets after normalization. Parameter correlations were examined to ensure stable convergence.

S6. Statistical-mechanical basis of the logistic isotherm

The logistic function employed to describe the surface-pressure isotherm arises naturally from a cooperative two-state statistical model. Each interfacial molecule can occupy either a low-density, disordered (gas-like) state or a high-density, ordered (condensed) state. The relative occupancy of these states follows Boltzmann statistics,

$$p(A) = \frac{1}{1 + \exp[(\Delta G(A))/k_B T]},$$

where $\Delta G(A) = G_2(A) - G_1(A)$ is the free-energy difference between the two configurations at molecular area A. Assuming $\Delta G(A)$ varies linearly with compression, $\Delta G(A) \approx \gamma(A - A_c)$,

the occupancy reduces to the logistic form

$$p(A) = \frac{1}{1 + \exp[(A - A_c)/A_t]},$$

with midpoint A_c corresponding to the area where both states are equally probable, and $A_t = k_B T/\gamma$ defining the sharpness of the transition. If the macroscopic surface pressure $\Pi(A)$ scales with the fraction of molecules in the condensed state, the isotherm follows directly as

$$\Pi(A) = \Pi_{\min} + \frac{\Pi_{\max} - \Pi_{\min}}{1 + \exp[(A - A_c)/A_t]},$$

which captures the cooperative condensation behavior observed in Langmuir monolayers.

S7. Surface pressure-area and surface potential-area isotherm of HET molecule

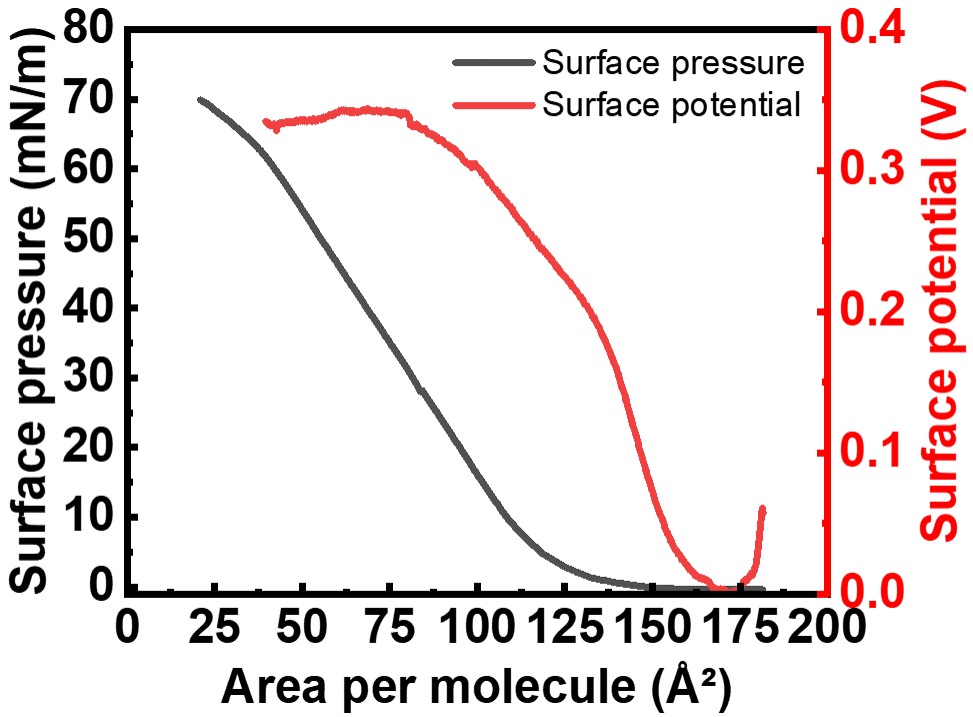

Figure S6: Surface pressure-area and surface potential-area isotherm of HET molecule

S8. Comparison of L-L and SL-L fitting

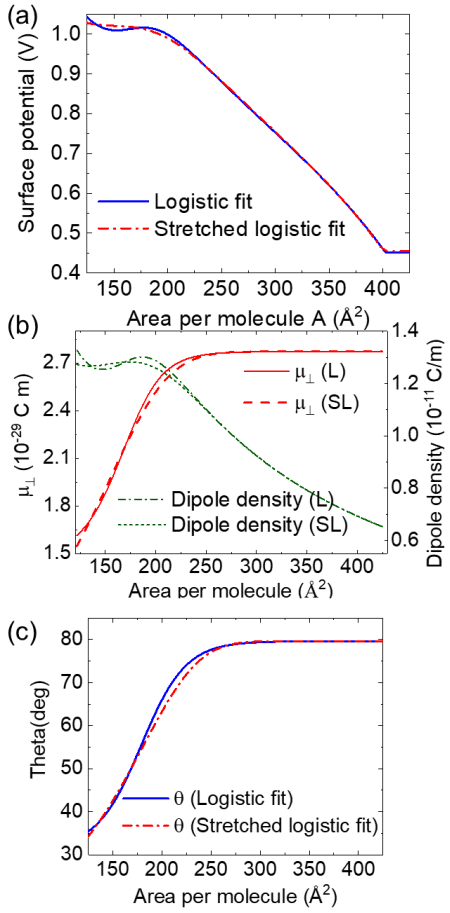

Figure S7: A comparison of the L-L and SL-L fitting: (a) fit to the surface potential data. (b) $\mu_\perp$ and dipole density, and (c) orientation of the molecular dipole, θ.

S9. Contact angle measurement

Figure S8: Contact angle measurement on LB monolayers of (a) HET-OXD and (b) HET on Si substrate.

References

(1) De, R.; De, J.; Gupta, S. P.; Bala, I.; Pandey, U. K.; Pal, S. K.; others Oxadiazole-integrated heterocoronene discotics as ambipolar organic semiconductors. *Journal of Materials Chemistry C* **2023**, *11*, 980–985.

(2) De, J.; Bala, I.; Gupta, S. P.; Pandey, U. K.; Pal, S. K. High hole mobility and efficient Ambipolar charge transport in heterocoronene-based ordered columnar Discotics. *Journal of the American Chemical Society* **2019**, *141*, 18799–18805.

(3) Marvin was used to optimize the geometry by running MMFF94 energy minimization. Marvin version 22.9, ChemAxon. https://www.chemaxon.com.

(4) Horcas, I.; Fernández, R.; Gomez-Rodriguez, J.; Colchero, J.; Gómez-Herrero, J.; Baro, A. WSXM: a software for scanning probe microscopy and a tool for nanotechnology. *Review of scientific instruments* **2007**, *78*, 013705.